Neural Plasma Reconstruction from Diagnostic Imaging

Ekin Öztürk[1], Rob Akers[2], Abhijeet Ghosh[1], Stanislas Pamela[2], Pieter Peers[3], The MAST Team[2]

[1] *Imperial College London, London, United Kingdom*

[2] *Culham Centre for Fusion Energy, Abingdon, United Kingdom*

[3] *College of William & Mary, Williamsburg, VA, USA*

Introduction

Experiments like MAST collect vast amounts of diagnostic data, among these imaging data of the plasma and impurity emissions captured by a high speed camera system. These high temporal resolution images can be used for plasma monitoring and control, but are underutilised due to the difficulties in estimating relevant plasma parameters such as the shape and composition from such images. To that end, we leverage a neural network to estimate the 2D distributions of neutrals, electrons and temperature from images of plasma obtained from the high speed cameras inside the MAST vessel.

Our networks infers the plasma parameters by learning the non-linear mapping between synthetic images of the plasma D-alpha emission and the distributions of the neutrals density, electron density and the electron temperature. These emissions are computed using the equation $n_n \times n_e \times \mathrm{PEC}\,(n_e, T_e)$ where PEC is the Photon Emissivity Coefficient obtained from ADAS[1]. Our networks are composed of an image encoder net that takes the high speed images and encodes them to a latent vector. We also introduce an optional subnetwork to provide encoded latent vectors of point sample measurements that can be concatenated to the encoded image latent vectors with the goal of incorporating other diagnostic measurements and further improving accuracy. This latent vector is then decoded to predict the inputs of our plasma generation model. The biggest contribution of our networks are in predicting the distribution of neutrals in the vessel which cannot be measured directly and requires expensive Monte Carlo simulations to estimate.

Data Generation and Network Training

With real image data it is difficult to curate a dataset for effective training of a neural network due to the large number of images and lack of measured reference. Thus we propose a plasma data generation model that represents the plasma densities and temperature through 36 parameters that samples a domain representative of MAST experiments.

We then combine the generated plasma data with computer graphics techniques to render photorealistic images of the interior of the MAST vessel as seen by the high-speed camera.

These renderings are created using the MAST CAD model loaded into the Mitsuba 2[2] rendering engine with the materials set to a conductor model with a reflectance of 0.08 and a roughness of 0.25, and the camera parameters matched to the real camera. The images are monochrome (as we are simulating the transport of 656.1nm wavelength light) and rendered at a resolution of 512 by 512 using a null-scattering implementation that incorporates emission[3].

With simulated images and corresponding parameter distributions available, we are able to train neural networks to learn the aforementioned mapping. The dataset is randomly split into training, validation and test sets with a 75%/12.5%/12.5% split. The training algorithm used is Adam with an initial learning rate of 10^{-3} and weight decay of 10^{-6} with all other parameters set to their default values as described in [4].

In order to leverage other available diagnostics in MAST, such as the Thomson Scattering measurements (which provide 1D profiles of n_e and T_e on the midplane), we incorporate point sample measurements of the training data, and train a variant of the *Image-Only* network to evaluate the effect of incorporating these measurements. This *Point-Sample* network differs from the *Image-Only* network in that it, in addition to the input image, also encodes and concatenates the point measurements into the latent vector. Both networks are trained using a weighted mean square error (MSE) loss over the normalized 36 parameters with weights selected to penalise discrepancies in the density and temperature scales.

Results

The *Image-Only* model achieves an unweighted MSE of 0.071 on the synthetic test set while the *Point-Sample* model achieves an unweighted MSE of 0.056 on the normalized parameters. While the test set errors are useful, we also look at the relative sum of errors in the predicted poloidal cross-sections as well as the relative sum of errors in the predicted profiles which are shown in Tables 1. Additionally, we take a representative sample from the synthetic test set and show in Figure 1 how the predicted profiles change between the two models.

In addition to the dataset errors, we also compare the errors of the network as applied to *real* measured data as part of the MAST experiment. Specifically, we look at shot 30305 which was chosen due to the high time resolution of both the camera and Thomson scattering measurements. Figure 3 shows the renders from the predicted poloidal cross-sections and Figure 2 shows a comparison of the density and temperature profiles for the same frame shown in Figure 3 corresponding to a time of 0.236026s. Figure 4a shows the absolute error and Figure 4b shows the relative sum of errors between the predicted profiles and the measured values over the duration of the shot.

Figure 2 also shows the neutrals density, and together with Figure 3, we see that the *Image-*

	Poloidal Cross-Section			Point Samples		
	n_n (%)	n_e (%)	T_e (%)	n_n (%)	n_e (%)	T_e (%)
Image-Only Model	54.0346	47.2957	47.7827	20.3681	20.1273	4.7822
Point-Sample model	52.7983	45.0586	13.7578	29.1160	19.1003	3.8448
Change	**1.2363**	**2.2370**	**34.0250**	-8.7479	**1.0269**	**0.9373**

Table 1: Relative Sum of Errors in the Poloidal Cross-Sections and the Point Samples corresponding to Thomson Scattering Measurements. Reduction in error is shown in **bold** and regressions shown in red.

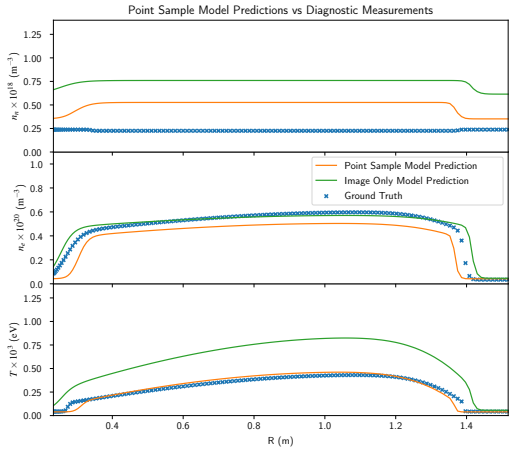

Figure 1: $Z = 0$ *Profiles computed from predictions of poloidal cross-sections made with the* Point-Sample *Model (Orange) and* Image-Only *Model (Green) compared to the Ground Truth profile (Blue crosses)*

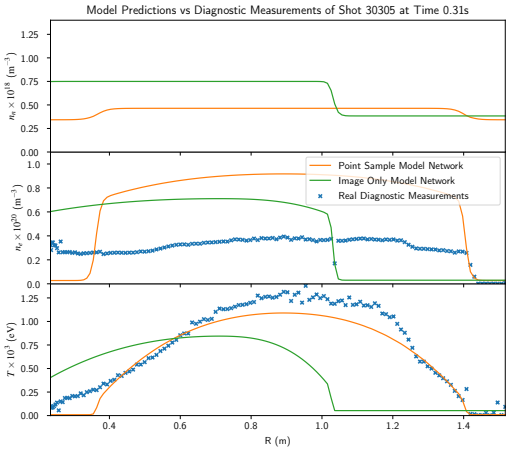

Figure 2: $Z = 0$ *Profiles computed from predictions of poloidal cross-sections made with the* Point-Sample *Model (Orange) and* Image-Only *Model (Green) compared to the Ground Truth profile (Blue crosses)*

Only model attempts to fit the gas puff emissions on the centre column. While the *Image-Only* model correctly ascertains that there is an increase in neutrals density somewhere, it misattributes this increase to an increase in core density. For future work, we intend to address this misattribution by providing the network with data that incorporates emissions due to neutrals density sources so that the network is better able to distinguish between the plasma equilibrium shape and composition and localised emissions.

Conclusion & Future Work

We have shown that our networks are successfully able to learn the nonlinear mapping between the images of the plasma emission and the cross-section profiles. Furthermore, we have demonstrated that providing the network with additional information in the form of point sam-

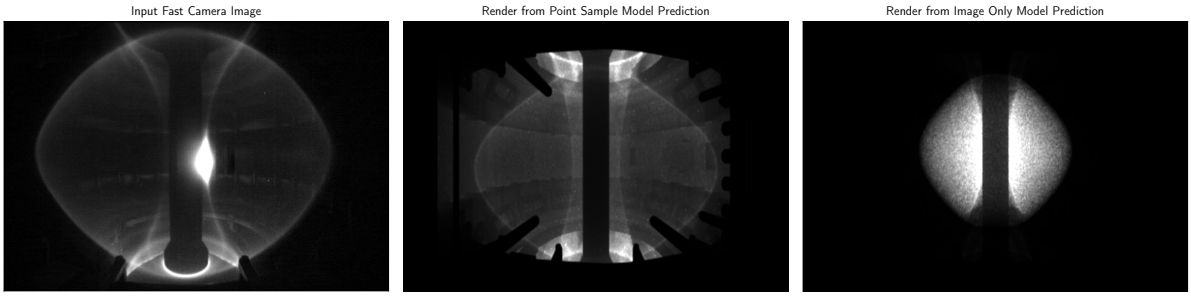

Figure 3: *Input Fast Camera Image (Left), Render from Predicted Poloidal Cross-Sections from* Point-Sample *model (Middle) and* Image-Only *Model (Right)*

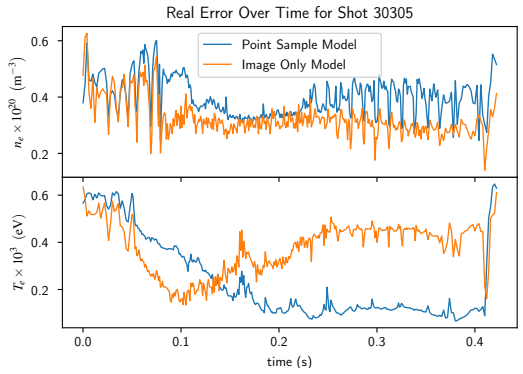

(a) *Absolute Error of the profile measurements at each frame time for the* Point-Sample *Model (Blue) and the* Image-Only *Model (Orange*

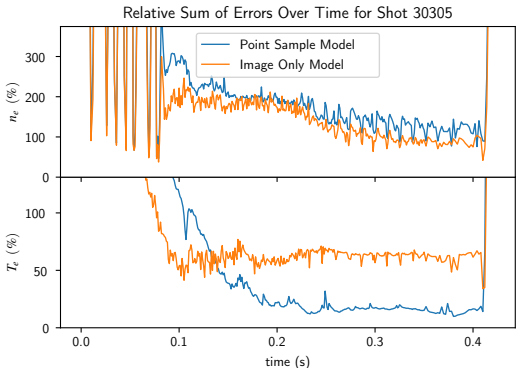

(b) *Relative Sum of Errors of the profile measurements at each frame time for the* Point-Sample *Model (Blue) and the* Image-Only *Model (Orange)*

ple measurements allows the network to better locate the plasma edge and better fit to the temperature. Importantly, our networks achieve these results without ever having seen real data in neither the training nor the validation sets, and by our results demonstrate that a network trained on purely synthetic data can generalize well to real world data. For future work, we would like to further investigate other network architectures as well as improve the networks' ability to correctly predict the scaling of n_n and n_e which are anti-correlated as seen in the emission equation.

References

[1] University of Strathclyde, "Open-adas." Online, 2021. Version 2.1. Retrieved on 30/06/2021.

[2] M. Nimier-David, D. Vicini, T. Zeltner, and W. Jakob, "Mitsuba 2," *ACM Transactions on Graphics*, vol. 38, pp. 1–17, nov 2019.

[3] B. Miller, I. Georgiev, and W. Jarosz, "A null-scattering path integral formulation of light transport," *ACM Transactions on Graphics*, vol. 38, pp. 1–13, jul 2019.

[4] D. P. Kingma and J. Ba, "Adam: A method for stochastic optimization," 2014.

Funding

Pieter Peers is partially supported by NSF grant IIS-190902